ADVANCED ENERGY & SUSTAINABILITY RESEARCH
Open Access
www.advenergysustres.com

Potential Application of Porous Oxide Ceramics and Composites in Concentrated Solar Technologies

Gözde Alkan, Peter Mechnich, Ferdinand Flucht, and Christian Willsch*

Concentrated solar thermal technology (CST) using solid particles as integrated thermal absorptance, transport, and storage medium offers higher storage densities and lower storage costs. In this application, ceramic particles are heated up rapidly in solar receivers up to 1000 °C and carried to the heat exchanger to generate hot air or steam. Hot and cold storage containers are used to store particles and transport tubes are needed to ensure the transportation of the hot and cold particles between CST plant components. There are various material properties needed to be fulfilled by these various CST components. High mechanical stability at elevated temperatures (>1000 °C), structural and mechanical stability after long time exposure to the heat, abrasion resistance against particle collisions, thermal shock resistance, chemical stability against particles are some of the most important properties. In this study, sintered bauxite particles, (Al_2O_3) matrix/(Al_2O_3) fiber, mullite matrix/mullite fiber ceramic matrix composites, plasma-sprayed alumina, and mullite ceramics are evaluated in terms of their mechanical properties and CST-related functional properties. Considering all properties, possible application as CST plant components are discussed and suggested.

1. Introduction

Concentrating solar technology (CST) is considered as one of the most promising renewable energy technologies, where solar irradiation is utilized for the production of electricity or process heat.[1] Through thermal energy storage (TES) integration, it is possible to overcome the off-sun condition drawback and achieve solar-to-electricity ratios.[2] Moreover, the need of higher operation temperatures for enhanced storage densities induced the development of solar particle technology in CST systems. Dark colored ceramic particles with high-temperature stability can be employed at 1000 °C and beyond as a direct solar hat absorber and storage medium to achieve higher storage densities with low maintenance costs.[3] In solid particle technology, the solar radiation is concentrated onto the direct absorption particle receiver, where the particles are heated up rapidly. Afterwards, hot particles are moving into the hot storage container until they will be transported, for example, to a steam generator to produce electricity in a steam turbine. Transportation to the cold storage follows the steam engine cycle. In on-sun conditions, particles are transported up to the receiver and the particle heating cycle is repeated again.[4,5] In order to achieve high efficiencies, proper material selection for the receiver, heat exchanger, storage tanks, and port-transport systems are crucial.

Oxide ceramic materials with porous structure such as ceramic matrix composites (CMC) promise high thermal shock resistance, excellent high-temperature stability and enhanced toughness with respect to dense ceramics. Many scientific and technological aspects of oxide CMC can be found in comprehensive literature overviews.[6,7] Thanks to their superior high-temperature properties, those materials are mainly developed for aerospace or industrial thermal processing applications.[8,9] A further class of oxide materials with high porosity and good thermal shock resistance are plasma-sprayed monolithic ceramics,[10] which nowadays find many applications in industrial thermal processes. In this study, however, both class of materials were evaluated and compared in terms of key properties for potential materials to build specific reactor components in concentrated solar power technology.

In the recent R&D project "Hotport", the German Aerospace Center (DLR) developed a new concept for a transportation and port system and elucidated the required properties in rotary kiln receiver furnace, newly developed transport systems and wall components, which are in contact with heated moving and falling particles for heated ceramic particles. Transport systems and solar receiver should endure high operation temperatures, fast cooling, and heating rates and have to endure mechanical stress when they are in contact with particles. Moreover, they should exhibit abrasion resistance and chemical stability against moving and falling heated particles. Heat storage walls should exhibit

G. Alkan, P. Mechnich, F. Flucht
German Aerospace Center
Institute of Materials Research
51147 Cologne, Germany
E-mail: goezde.alkan@dlr.de

C. Willsch
German Aerospace Center
Institute of Future Fuels
51147 Cologne, Germany

The ORCID identification number(s) for the author(s) of this article can be found under https://doi.org/10.1002/aesr.202400252.

DOI: 10.1002/aesr.202400252

chemical stability against the solid particles to prevent the sticking and agglomeration of the particles. In all cases, a certain amount of porosity is required to ensure minimize heat losses. To meet specific demands of aforementioned CST components, four key properties were determined as; thermal shock resistance, chemical stability, particle erosion resistance, and mechanical endurance in as-received state and after long-term operation.

Commercial plasma-sprayed alumina and mullite ceramics with intrinsic process-related porosity and porous, filament-wound alumina fiber-reinforced alumina matrix composites and mullite fiber-reinforced mullite matrix composites were examined in terms of those four key criteria in a comparative manner. Microstructural investigation was used to discuss the distinct properties of four candidates. Assessment of the commercial materials considering the CST-related criteria were performed and the most promising candidate material for this specific system component in CST plants was proposed.

2. Results and Discussion

2.1. Evaluation of Mechanical Properties and Microstructures

Mechanical endurance after long time exposure to high operation temperatures is a key material property for solar receiver and transport tubes. In order to rate the applicability of different ceramic materials in the envisaged environment, that is, relative short periods at very high as well as long-term dwell times at moderate temperatures, flexural strength of the as-received and thermally aged samples were determined by three-point bending tests, as represented in **Figure 1**.

In the as-received condition, ≈30 and 13 MPa strength were measured for PS-A and PS-M, respectively, well reflecting the general superior mechanical properties of Al_2O_3 versus mullite. After isothermal aging at three conditions (1200 °C–100 h, 1300 °C–250 h, and 1400 °C–50h), both materials exhibit significantly increasing room-temperature bending strengths up to the

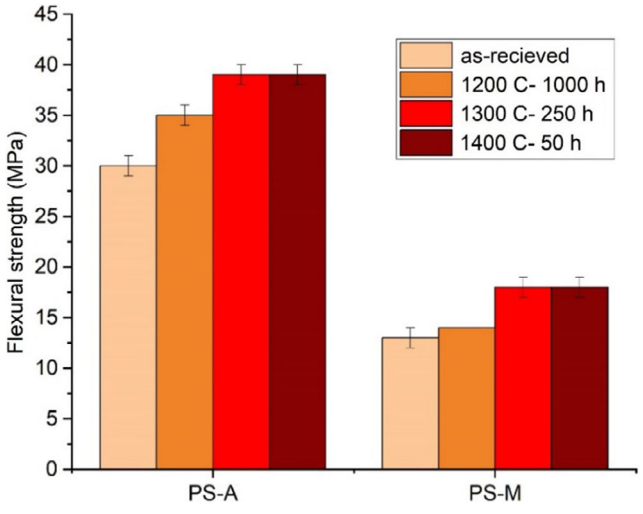

Figure 1. Flexural strength of PS-A and PS-M in as-received state and after thermal aging.

1300 °C–250 h condition (PS-A + 27%, PS-M + 23%). The quasi constant values at 1400 °C–50 h indicate that both materials already reached some kind of stable condition. Figure 6 represents the detailed microstructure of PS-A and PS-M materials in as-received condition and after thermal aging at 1400 °C–50 h, respectively.

SEM microstructures in **Figure 2** show different effects associated with further sintering of PS-A (a, b) and PS-M (c, d). PS-A exhibits disappearance of grain boundaries and nanopores, that is, re-crystallization and sintering. The microstructure of PS-M is evolving more significantly, evidently s precipitation of brightly contrasted small grains, which could be identified as pure Al_2O_3, took place. Moreover, formation of some nanopores is visible. On the contrary, there is an obvious sintering effect with partial bridging of cracks. It can be said that the total of sintering effects is more favorable in the case of PS-A, as also indicated by relative more increasing mechanical strength. Density measurements are also in parallel with SEM and mechanical test findings. PS AA exhibited an initial density of 3.32 g cm^{-3} which slightly increased to 3.33 and 3.34 g cm^{-3} after 1200 and 1300 °C annealing, respectively. For PS the MM initial density was 2.70 g cm^{-3}, which remained constant after thermal storage at 1200 and 1300 °C, that is, possible densifications were below the detection limit. Mechanical properties of CMC-AA and CMC-MM materials were also tested in as-received state and after all thermal aging conditions. Flexural strength in the fiber dominating test orientation for both CMC materials are given in **Figure 3**.

In the as-received state, CMC-AA exhibits the highest flexural strength around 250 MPa. CMC-MM has relatively lower strength around 150 MPa. However, CMC-AA and CMC-MM exhibit quite distinct thermal aging behavior. CMC-AA loses significantly strength (≈−74% after 1350-250h; −78% after 1400 °C–50 h) to even comparable values with plasma-sprayed PS-A (see Figure 1). The mechanical strength of CMC-MM is decreasing much less (≈−17% after 1350–250h; −30% after 1400 °C–50 h), with remains relatively stable after all thermal aging conditions. It is noteworthy that after exposure to each of the thermal aging conditions, CMC-MM exhibited higher strengths than CMC-AA despite its much higher as-received strength. In order to elucidate this distinct behavior of two materials, thermally aged CMC-AA and CMC-MM were analyzed by SEM. Micrographs given in **Figure 4** reveal a dramatic change in the thermally aged CMC-AA material.

In Figure 4a, it is possible to observe the overall smaller matrix grain size and the higher matrix porosity. The detail image in Figure 4c reveals the abnormal crystal growth and associated degradation of Nextel 610 fibers and also evidence for strong sintering and growth of matrix Al_2O_3 grains, as previously reported.[11] After thermal aging at 1200 and 1300 °C, density of CMC AA increased from the as-received density of 2.6 g cm^{-3} to 2.65 and 2.73 g cm^{-3}; respectively. For the CMC MM, this densification effect after thermal storage is relatively less than AA. As-received density of MM 2.49 g cm^{-3} was slightly increasing to 2.50 and 2.53 g cm^{-3} after thermal storage at 1200 and 1300 °C, respectively. This is easily explained by the lower sintering activity of the mullite matrix. The significant sintering after thermal aging for CMC samples with respect to PS and the

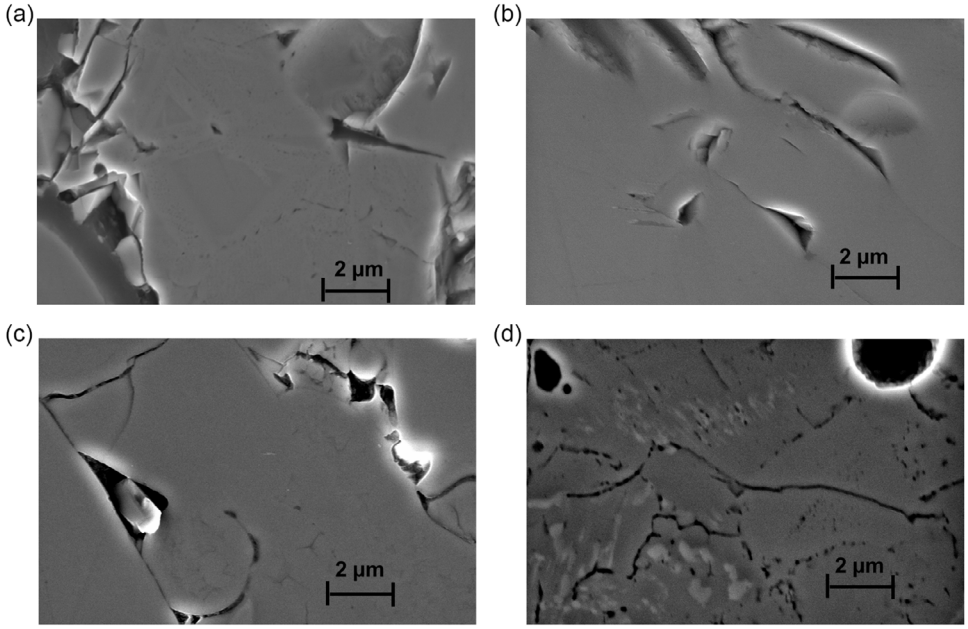

Figure 2. SEM microstructures of a) PS-A as-received b) after 1400 50 h c) PS-M as-received d) after 1400 50 h.

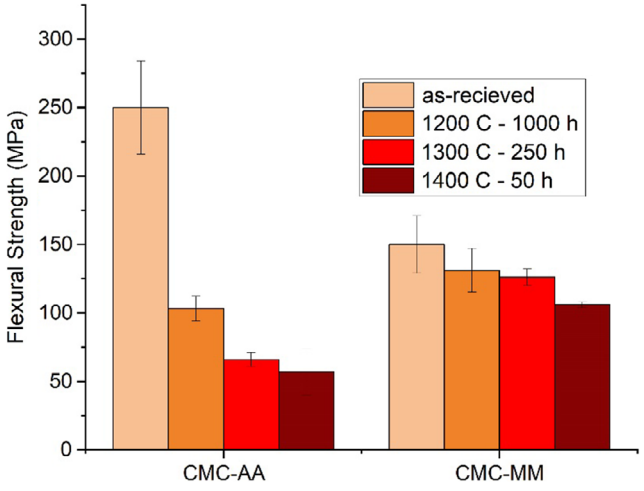

Figure 3. Flexural strengths of CMC-AA and CMC-MM in as-received condition and after thermal aging.

relatively constant behavior of PS-MM are consistent with the microstructural findings and mechanical test results.

This effect is commonly explained by out-diffusion of a SiO_2 dopant, which is added to the fiber in the range of 0.5 wt% to act as stabilizer at Al_2O_3 grain boundaries.[12] Such kind of microstructural effects, triggered by thermally activated diffusion, are responsible for the fact, that the aged CMC-AA materials behave rather like weak monolithic ceramics rather than fiber-reinforced composites, which results in measured poor mechanical properties in Figure 7. Regarding the CMC-MM, it exhibits a relatively stable microstructure with less pronounced matrix sintering as well as much less degradation of the Nextel 720 fibers. In this case, the binary fiber microstructure of mullite enclosing acicular Al_2O_3 grains provides mutual inhibition of excessive crystal growth, which is supported also by a relatively lower diffusivity and grain growth activity of mullite. Due to the high temperature and long-term stable microstructure of mullite matrix and fibers, CMC-MM can retain much more of their mechanical properties after thermal aging.

A further relevant property of possible CST container wall materials is strength at high temperature. Although a detailed and comprehensive experimental campaign was beyond the scope of this study, we performed additional high-temperature experiments being at least indicative for the assessment and ranking of materials. For the measurements three as-received bending bars of each material were heated with 20K min^{-1} to the test temperature, and kept for 5 min to equilibrate. **Figure 5** presents the results of 3-point bending tests performed at 900 and 1200 °C, respectively. The HT-bending strengths reflect the general trends observed at RT, but again with noteworthy aspects. In case of the PS-materials, PS-A bending strengths are retained by about 80% at 900 °C and 75% at 1200 °C, respectively. The corresponding values of PS-M are significantly better, about 92% at 900 °C and 85% at 1200 °C. A striking difference is observed for the CMC materials: at 900 °C, CMC-AA retain only about 59% of their RT strength, which is further drastically deteriorating to about 17% at 1200 °C. The behavior of CMC-MM is completely different, they retain about 98% of their strength at 900 °C, and about 93% at 1200 °C. As in short-term HT-bending experiments no significant aging, that is, microstructural evolution is expected, the only plausible reason for the observed strong differences between Al_2O_3 and mullite materials is the onset of thermally activated diffusion and related effects. In particular creep caused by slip systems and gliding of grain boundaries is a phenomenon typical for α-Al_2O_3, whereas mullite and mullite ceramics are well known for their microstructural stability at high-temperature. Although the initial properties of CMC-AA are

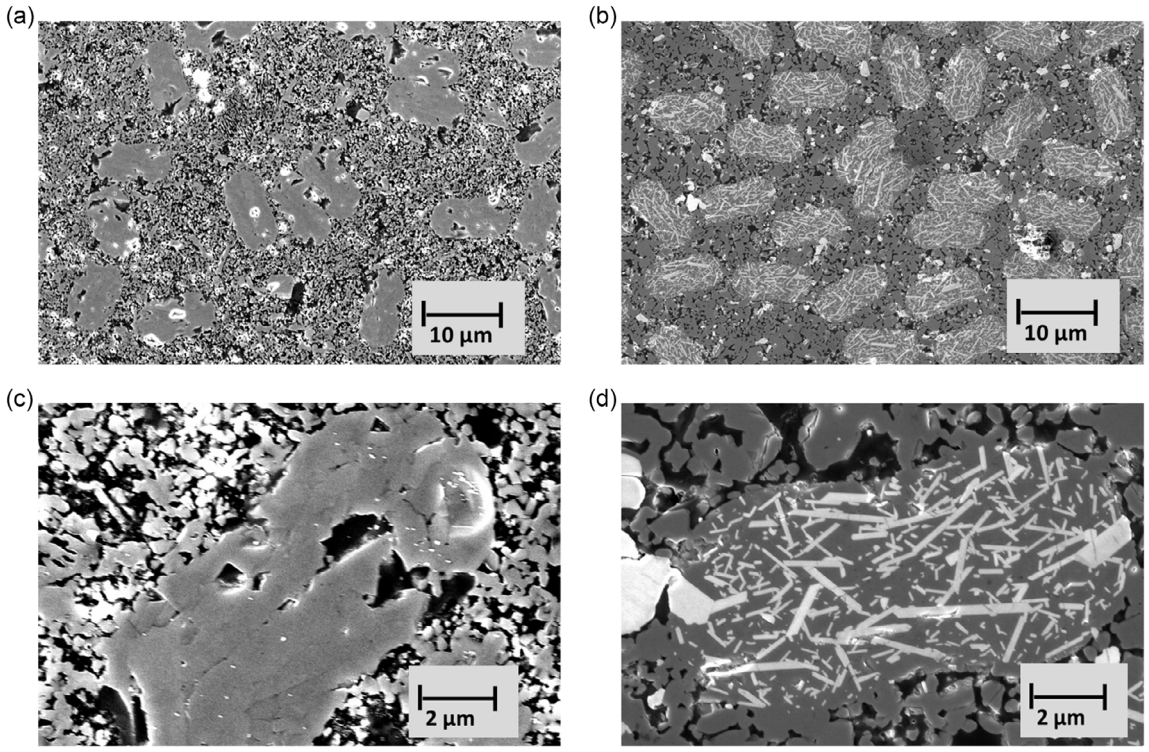

Figure 4. SEM microstructure of a) CMC-AA and b) CMC-MM after 250 h at 1300 °C and detail views of the c) Nextel 610 alumina and d) Nextel 720 mullite/alumina fibers.

outperforming those of CMC-MM, the relative thermal stability of the latter makes it the preferred candidate for the envisaged applications. In any case, plasma-sprayed ceramics exhibit relatively poor mechanical properties, which makes their utilization in the envisaged CST application, that is, as wall materials for moving transport containers, questionable.

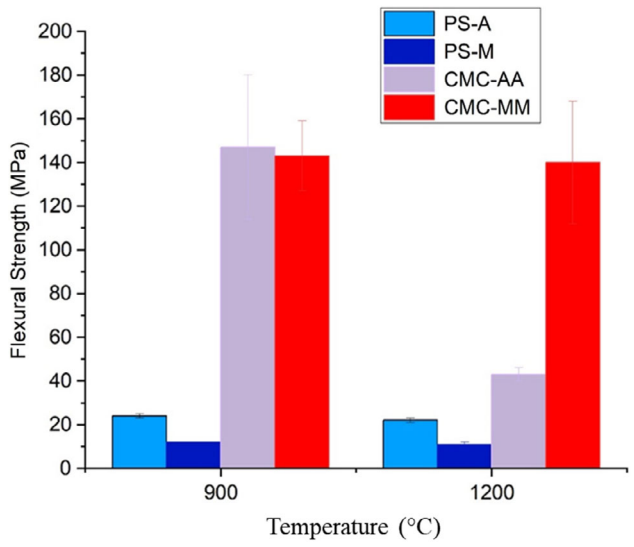

Figure 5. Flexural strength of CMC and PS materials measured by 3-Point bending at 900 and 1200 °C.

2.2. Assessment of CST-Specific Materials Properties

Beyond mechanical properties, system component materials have to exhibit desired CST technology related material properties such as chemical inertness, particle abrasion resistance, and solar thermal shock resistance.

2.2.1. Sintered-Bauxite Particles and Chemical Stability against CMC

The main scope of this study is the ranking and assessment of the structural components to be used in solid particle technology. However, for an efficient CST plant with enhanced energy storage densities, a well selection on particle type is also crucial. Bauxite proppants, actually produced for fracking and oil industries, are considered as state-of-the art in particle technology thanks to their good spherical form and high-temperature stability.[13,14] Sintered bauxite (SB) proppants from Saint Gobain were used to evaluate chemical stability of ceramic components and abrasion resistance (this section and section 2.1) Solar absorptance is one of the most important properties and a minimum solar weighted absorptance (ASTM 173d) of 0.8 is crucial in particle technology. Depending on the chemical composition, especially amount of iron bearing oxides, commercial proppants exhibit a scattering solar absorptance between 0.80 and 0.95.[14] The absorptance spectra of SB from Saint Gobain, focus of this study, in the range of 320–2500 nm is given in **Figure 6**. The solar weighted absorptance of proppants was determined as 0.82.

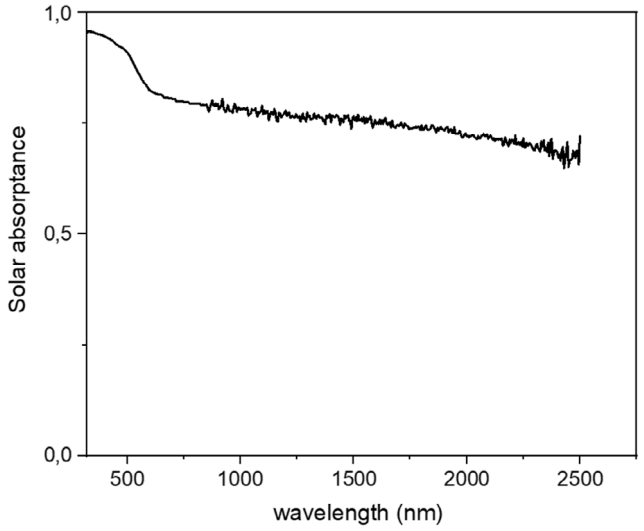

Figure 6. Solar absorptance of sintered bauxite (SB) particles measured by spectrometry.

Beyond material and functional properties, techno economic analyses and estimation of levelized cost of electricity (LCOE) are also critical. In previous studies, 12.7 € kWh^{-1} specific storage cost and 0.844 € kg^{-1} particle break-even costs were estimated for such kind of sintered bauxite proppants.[15]

Chemical stability is crucial for all system wall components (solar receiver, transport, storage) which are directly in contact with solid particles. Especially at elevated temperatures, reaction between particles and wall components would result in piling up of the particles within the component and would inhibit further particle flow.

The possible chemical interaction between sintered bauxite particles and ceramic wall materials was studied experiments where particles were placed on top of CMC-AA and CMC-MM plates and annealed at high temperature. Whereas annealing at 1000 °C did not lead to significant effects, after one week of isothermal annealing with sintered bauxite particles at 1300 °C, some of the particles stacked to the CMC surface indicating onset of chemical interaction, as can be seen in **Figure 7**a.

Figure 7b shows a representative SEM micrograph of particle/CMC-AA interaction cross-section. It is possible to observe original CMC microstructure, where alumina fibers can be distinguished from alumina matrix, around 80–100 µm below the surface. As approaching to the substrate surface, where it is in close contact with the bauxite particle, an alteration from the original microstructure can be detected (Figure 7c).

Similar to the CMC-AA, a different morphology was observed at beneath the surface of CMC-MM, where it is in contact with the particle. In the parts deeper than 100 µm, unreacted original MM morphology can be observed, where fibers and matrix are clearly discernible. Since the chemical interaction takes place in a very thin zone (≈100 mm), substantial crystal phase changes are not anticipated. The observed effect is due to the partial melting of bauxite particles and wetting of close particles. In order to understand the chemistry of the interaction zone better, EDS analysis was performed in microstructurally altered zones as indicated in Figure 6, **8**.

Here it is worth to mention that bauxite particles are consisting mainly of corundum (α-Al_2O_3), iron rich, mostly spinel-type crystals, and a glassy phase.[7] Therefore, they contain Al, Si, Fe and some glass former elements like Mg and K. **Table 1** indicates that CMC-AA includes beneath the surface additional Si and Fe, which are not present in the as-received state and have diffused

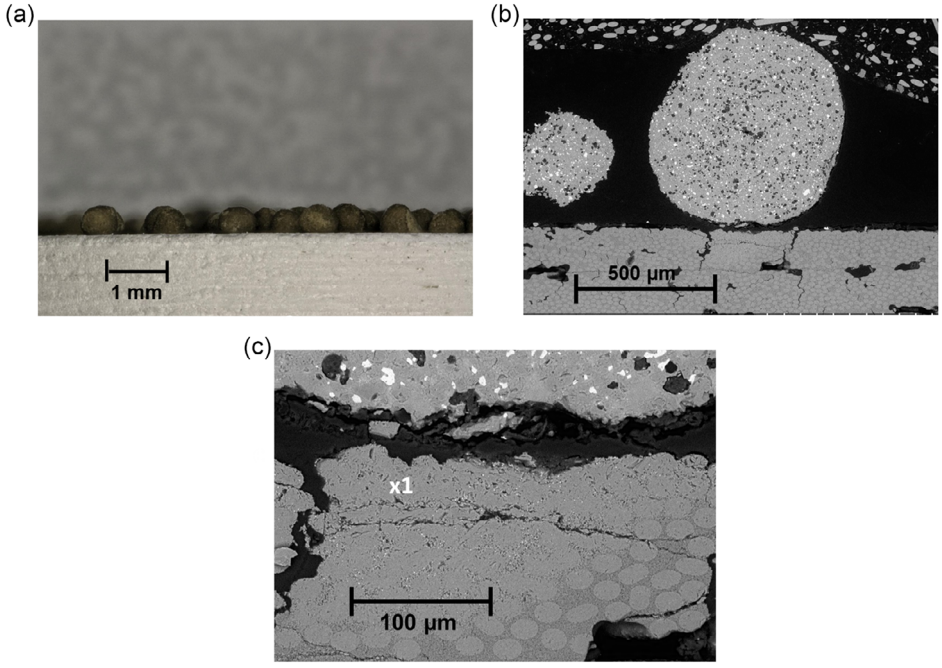

Figure 7. a) Visual appearance and b) SEM micrograph of bauxite particle/CMC-AA substrate contact cross-section. c) Details of the chemical interaction zone.

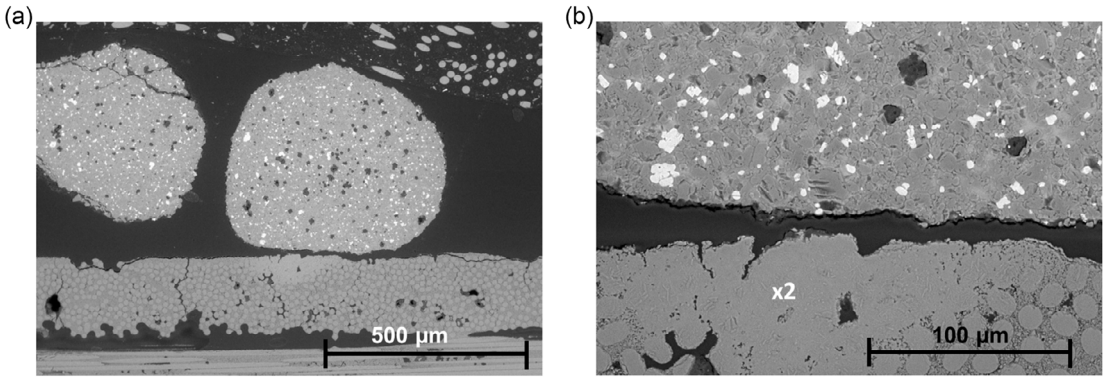

Figure 8. a) SEM micrograph of bauxite particle/CMC-MM substrate contact zone. b) Close-up of the chemical interaction zone.

out of the bauxite proppants. Alumina fibers contain 0.3 wt% SiO_2 and 0.5 wt% Fe_2O_3 in the as-received condition. These values increased up to 1.3 and 0.9 wt%, as listed in Table 1 as well as the different morphology indicate the inward diffusion from additional Fe, Si from bauxite particles. Similarly, in the case of mullite, Fe and glass phase components' diffusion were revealed. These SEM/EDS analyses show that there will be an around 100 µm wide chemical interaction zone at alumina/mullite ceramic walls covered with bauxite particles after 1-week static storage at 1300 °C, which is considered only minor relevant regarding a typical total wall thickness of 3 mm. After very long-term high-temperature exposure, nucleation and growth of new crystalline phases cannot be ruled out, but this scenario could not be observed in this work. The behavior of PS-A and PS-M will evidently be similar to the CMC materials, i.e., both alumina and mullite ceramic walls can be considered as sufficiently chemically stable for bauxite-type particle-based CST applications; keeping in mind that envisaged real operation temperatures of 1000 °C are much lower.

2.2.2. Resistance against Particle Impact/Erosion

Particle impact and erosion resistance are crucial for the system components which are in contact with moving, i.e., rolling, sliding, and falling particles. Upon hitting and friction of the moving particles, surface of the system components should exhibit negligible debris formation due to the abrasion/erosion. This is especially important for solar receiver and transport tubes.

Erosion resistance of the substrates were tested at room temperature by the resonance acoustic mixing (RAM) method using the sintered bauxite particles. The substrate plates are placed as cover of a tubular plastic container and fixed in the sample holder of the RAM. Particles inside the container are accelerated by the specific vertical RAM motion with 100 g-force and hit the free-standing substrate surfaces where they create collision damages. Cumulated weight losses are recorded and used as measure for the relative particle impact resistance of investigated materials as given in **Figure 9**.

In these experiments, a monolithic and fully dense Al_2O_3 ceramic plate (C799 type) was used as a reference material, which exhibited almost no weight loss due to its quasi pore-free microstructure. In comparison with dense Al_2O_3, all tested substrates experience significant mass losses with increasing particle exposure time. Both plasma spray ceramics exhibited a much better resistance than both CMC materials, as can be seen in Figure 4. The superior behavior of PS-A and PS-M is explained by their relative low porosity: whereas PS-A has a density of $\rho = 3.32\ g\,cm^{-3}$, corresponding to 84% of the theoretical density (TD) of α-Al_2O_3 ($3.95\ g\,cm^{-3}$), PS-M with $\rho = 2.69\ g\,cm^{-3}$ reaches about 86% of the TD of stoichiometric mullite ($3.15\ g\,cm^{-2}$). Thus, the slightly higher porosity of the PS-A microstructure can be related to its slightly worse particle erosion resistance. The relative low bulk densities of $2.41 g\,cm^{-3}$ (CMC-AA) and $2.49\ g\,cm^{-3}$ (CMC-MM) can easily explain their low erosion resistance. However, it must be emphasized that their

Table 1. Point EDS analysis of the chemical interaction zones between CMC-AA and CMC-MM with bauxite particles.

at.%	O	Al	Si	Fe	Mg	K
#1 (Figure 6)	57.3	40.5	1.3	0.9	–	–
#2 (Figure 7)	59	29.7	9.4	0.9	0.3	0.4

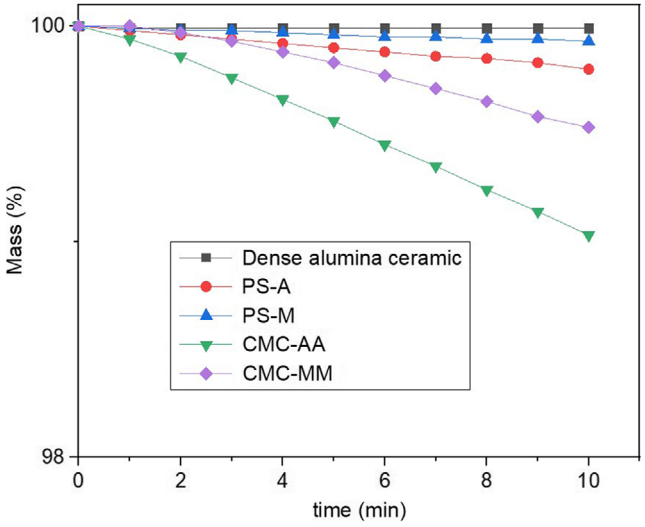

Figure 9. Mass loss of ceramic substrates due to the abrasion after RAM tests with bauxite particles.

microstructures consist of 'strong', i.e., fully dense fibers and 'weak' matrices with even higher porosity. It is evident, that such highly porous matrices are prone to particle erosion and are the weak point in terms of CMC erosion resistance. Although the bulk densities of CMA-AA and CMC-MM are similar, a simple estimation yields a much lower relative density of CMC-AA (about 61% TD of Al_2O_3) compared to CMC-MM (about 73% TD of a fictional 2:1 mullite/α-Al_2O_3 mixture). Consequently, the relatively faster erosion of the CMC-AA material is explained by its much higher matrix porosity (compare also microstructures in Figure 8a,b), resulting in an overall lower matrix strength.

2.2.3. Solar Thermal Shock Resistance

In CST technology focused in this study, through concentrated solar radiation the particles are being heated up to 1000 °C within a few seconds in solar receiver and these heated particles will be falling through the transport systems. Solar receiver and transport components have to endure the stresses created through this high temperature gradient without experiencing catastrophic fracture. In particular thermal shocks generated by irradiation with focused sunlight are considered critical.

In order to assess the thermal shock resistance of different materials in a qualitative manner, experiments with very high heating rates and resulting thermal gradients were performed in DLR´s solar furnace. Disk shaped samples (d 50 × h 3 mm) were coated on one side by using black Pyromark paint in order to provide high absorptance of focused sunlight; thereby very fast solar furnace heating of samples to very high temperature is achieved. A typical heating run was performed during 10 s. After tests, macro examination revealed the partial melting of the samples, indicated by their glassy appearance and formation of ≈20 mm wide holes in the center, except of the plasma-sprayed Al_2O_3 disk where only melting was observed. Here it is worth to emphasize that this may be a coincidence. PS-A has also partially melted and in the case of a few seconds longer exposure to the concentrated solar light, it could have also exhibited a hole. The diameter of the holes is evidently reflecting the size of focal area, i.e., the circular hot-spot with quasi homogeneous temperature distribution, which was also detected by an IR camera as about 20 mm. The local highest reached temperatures were estimated using the melting temperature of alumina and mullite as 2050 and 1850 °C, and the outer regions of the disks remained typically in the range of 200 °C, linear radial temperature gradients of about 800 and 900 K cm^{-1} can be estimated for Mullite and Al_2O_3 materials, respectively. Despite the local melting of the samples, none of the substrates experienced catastrophic fracture. Details of the damaged surfaces after thermal shock test were investigated by low vacuum SEM as represented in **Figure 10**.

Large cracks are observed in the case of PS materials (Figure 10a,b) starting from the hot-spot zone, but also some branching into smaller cracks perpendicular to the main crack are observed. However, as no full shattering of the plates occurred, significant energy dissipation provided by the porous microstructures of PS-materials is assumed. In the case of both CMC materials, cracks also initiated from the edges of the focal holes, but were clearly deflected by the ceramic fibers. Owing to the pronounced crack deflection, further crack propagation was inhibited within 4-5 mm as can be seen in Figure 9c,d. Materials with similar structure, PS-A and PS-M, as well as CMC-AA and CMC-MM, exhibits similar damage tolerance after thermal shock

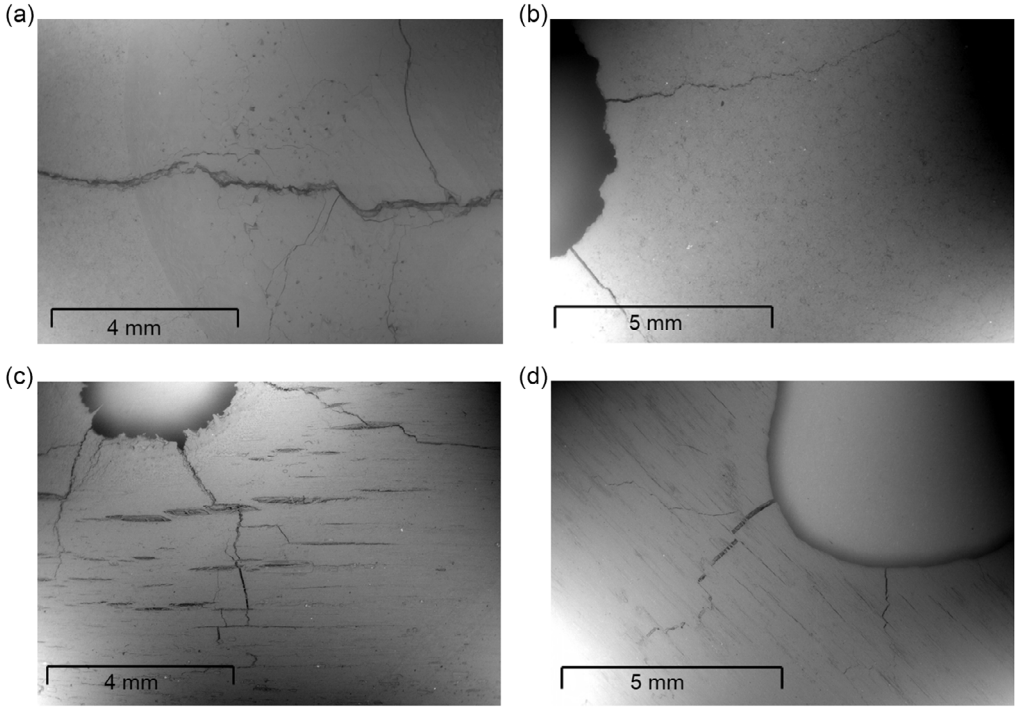

Figure 10. SEM analysis of damaged samples after thermal shock tests in solar furnace: a) PS-A, b) PS-M, c) CMC-AA, and d) CMC-MM.

Table 2. Possible application of candidate materials in various parts of CST systems.

	Candidate materials (in the appropriate order)
Receiver	CMC MM-RBAO
Transport	CMC AA RBAO, CMC MM RBAO
Storage	PS-A, PS-M, CMC AA, CMC MM

tests, independent from their chemistry. It is worth to mention that, densely sintered monolithic alumina, tested in identical conditions for the comparison purposes, exhibited a catastrophic fracture when the temperature gradient between the center and the outer regions of the sample was only around 200 °C. Pores in the structure of plasma-sprayed ceramics and the fibers of CMCs contributed to the inhibition of crack propagation, which makes both types of material thermal shock resistant.

2.3. Consideration of Oxide Ceramics and Oxide CMC for Envisaged Application in CST

Table 2 represents possible use cases of four assessed candidate materials in CST technology. To sum up, all materials exhibit good thermal shock resistance and sufficient chemical stability. Particle erosion resistance of both types of plasma-sprayed ceramics was acceptable, whereas the performance of both CMC types was inferior. However, in a previous study, we have demonstrated that reaction bonded alumina coatings (RBAO, note also mark-up in Figure 10) at CMC surfaces can enhance particle erosion resistance to a level comparable with dense materials.[16] Therefore, both plasma-sprayed ceramics and RBAO-coated CMC materials are considered suitable in terms of particle erosion resistance desired for this specific CST application. Room temperature mechanical strength of plasma-sprayed materials makes their use impracticable in mechanical strength requiring components, that is, receiver, transport tubes and CMC materials remain as preferred candidates. For solar receiver, the determining property is their high temperature and long-term endurance, which was assessed by their mechanical strength levels at high-temperature and after thermal aging. Despite their high as-received mechanical strength, significant loss of strength of the CMC-AA materials and much less deteriorating mechanical properties of CMC-MM materials, makes CMC-MM the best compromise to be used as receiver component in CST application, where mechanical endurance is crucial. For the transport tubes, long terms exposure to the high heat is not the case; therefore, CMC AA or MM can be used thanks to their promising thermal shock resistance, mechanical endurance, when their abrasion resistance is enhanced by RBAO coating. Considering the chemical stability, it is possible to use all four candidates in storage tanks.

3. Conclusions

Four different commercial materials; plasma-sprayed (PS) alumina and mullite, alumina fiber reinforced/alumina matrix and mullite fiber reinforced/mullite ceramic matrix composites (CMC); were examined together with sintered bauxite particles in order to evaluate their potential application as concentrated solar thermal (CST) system components such as solar receivers, transport tubes and storage tanks. As-received mechanical properties of plasma-sprayed materials are significantly low (10–20 MPa); therefore, their use as wall component is not plausible. The highest as-received strength was measured for alumina-based CMC around 250 MPa but after thermal aging it loses strength down to 60 MPa. Despite its significantly lower initial strength, mullite-based CMC mechanical strength is almost not affected from thermal aging. Microstructural investigation showed important matrix sintering, fiber crystal growth and degradation for the alumina-based CMC material, which were much less pronounced for the mullite-based CMC. Both alumina and mullite materials exhibit also high-temperature stability against the state-of-the art sintered bauxite particles. Due to the high porosities in their structure, PS and CMC materials exhibit poorer particle erosion resistance when compared with dense ceramics. Thanks to their crack deflection mechanisms by pores and fibers, all exhibit high damage tolerance and thermal shock resistance Owing to superior high temperature microstructural stability, mullite-based CMC have the most promising long term and high temperature mechanical properties and suggested to be used as solar receiver and transport components. All four candidates can be considered as promising for the storage tanks and component walls thanks to their good chemical stability against sintered bauxite particles.

4. Experimental Section

Commercial plasma sprayed PlasCera alumina (PS-A) and mullite (PS-M) ceramics were obtained from LWK Plasma Ceramics (Wiehl, Germany) and commercial WHIPOX alumina fiber reinforced/alumina matrix (CMC-AA) and mullite fiber reinforced/ mullite matrix ceramic composites (CMC-MM) were obtained from WPX Faserkeramik GmbH (Troisdorf-Spich, Germany). Employed oxide fibers are Nextel types 610 (CMC-AA) and 720 (CMC-MM) with 10K Den bundles (3M, USA)). In terms of winding pattern, the fiber orientation is $+/-45°$. From SEM cross sections a plausible fiber volume content of 35–40% can be estimated. All examined samples from both type of materials were double-side machined plates with a thickness of 3 mm. In as-received condition CMC AA, CMC MM, PS-A and PS-M exhibit densities of 2.6, 2.49, 3.32 and 2.70 g cm^{-3} respectively. Thermal conductivity of PS- A is 3.5 and 1 W mK^{-1} at RT and 1200 °C; respectively. PS-M has a lower thermal conductivity at room temperature 1.2 W mK^{-1} but at 1200 °C same with PS-A; 1 W mK^{-1}. In the case of CMC materials; AA has a thermal conductivity of 5.8 W mK^{-1} @ RT and 2.35 W mK^{-1} @ 1300 °C MM has relatively lower thermal conductivity of 1.8 W mK^{-1} at RT and 1.3 W mK^{-1} @ 1300 °C. Thermal aging of CMC and PS materials was conducted in muffle furnaces at three different conditions; 1400 °C for 50h, 1300 °C for 250 h and 1200 °C for 1000 h; respectively.

Sintered-bauxite particles with average diameter of about 1 mm (Saint Gobain, Courbevoie, France) were used as reference state-of-the art materials to investigate chemical stability of CMC and PS materials in simulated operation thermal conditions. The particles have a bulk chemical composition of $Al_2O_3 > 75$ wt%, $SiO_2 < 10$ wt%, (Fe_2O_3, TiO_2) < 5 wt%. Particles were placed on top of the CMC and PS plates and stored isothermally in a muffle furnace at test temperatures for one week, respectively. Particle–substrate interaction cross-section was analyzed by SEM/EDS in terms of microstructure and chemistry.

A resonance acoustic mixer 'RAM' (LabRAM-II, Resodyn, Butte, MT, USA) was utilized to test impact resistance of samples against the bauxite particles. A detailed description of the test method can be found

elsewhere.[13] Flexural strength of ceramic materials was determined by room- and high-temperature three-point bending test (10 × 50 mm bars; 25 mm span) using a spindle-driven test system (UTS, Zwick-Roell, Germany). 5 samples were measured for each material and condition. Thermal shock resistance of the samples was examined by hot-spot tests in the solar furnace at the DLR-Institute for Future Fuels, Cologne. Actual temperatures of the samples were not measured during the thermal shock experiments, samples were heated until hearing their cracking/fracture.

Cross-sectional microstructural analyses were performed by scanning electron microscopy (SEM; Ultra 55, Zeiss, Wetzlar, Germany). Digital optical microscopy (VHX 1000; Keyence Deutschland GmbH, Germany) was used to reveal the appearance of ceramic substrates and bauxite particles after thermal storage Surface investigations were performed by SEM in low vacuum condition (SU 3800, Hitachi High-Tech Europe, Krefeld, Germany).

Acknowledgements

This research is performed thanks to the EFRE NRW HOTPORT Project (0801589).

Conflict of Interest

The authors declare no conflict of interest.

Author Contributions

Gözde Alkan: conceptualization (equal); formal analysis (equal); investigation:lead; methodology (equal); writing—original draft:lead; writing—review and editing (equal). **Peter Mechnich**: conceptualization (equal); data curation (equal); investigation (supporting); methodology (equal); writing—original draft (equal); writing—review and editing (equal). **Ferdinand Flucht**: data curation (supporting); investigation (supporting); methodology (supporting). **Christian Willsch**: data curation (supporting); investigation (supporting); methodology (supporting).

Data Availability Statement

The data that support the findings of this study are available from the corresponding author upon reasonable request.

Keywords

ceramic matrix composites, ceramics, concentrated solar thermal

Received: August 16, 2024
Revised: October 28, 2024
Published online:

[1] A. Palacios, C. Barreneche, M. E. Navarro, Y. Ding, *Renewable Energy* **2020**, *156*, 1244.
[2] I. Sarbu, I. C. Sebarchievici, *Sustainability* **2018**, *10*, 191.
[3] A. Calderón, C. Barrenech, A. Palacios, M. Segarra, C. Prietto, A. Rodriguez-Sanchez, A. I. Fernandez, *Energy Storage* **2019**, *1*, e63.
[4] F. Nie, F. Bai, Z. Wang, X. Li, R. Yang, *EcoMat* **2022**, *4*, e12207.
[5] L. Amsbeck, B. Behrendt, T. Prosin, R. Buck, in *20th Solar Power and Chemical Energy Systems Conf.*, Solar PACES, Bejing, China **2014**.
[6] K. K. Keller, G. Jefferson, *Composites*, John Wiley & Sons, Inc., New Jersey **2014**.
[7] *Ceramic Matrix Composites*, (Ed: W. Krenkel), Wiley-VCH Verlag Gmbh & Co, KGaA, Weinhein **2008**.
[8] J. Lincoln, B. Jackson, B. A. Barnes, A. Beaber, A. L. Visser, *Advances in High Temperature Ceramic Matrix Composites and Materials for Sustainable Development, Ceramic Transactions*, (Eds: S. Mrityunjay, O. Tatsuki, D. Shaoming, K. Dietmar, S Kiyoshi, C. Bernd, H. Bernhard, A. Jun), Wiley **2017**, Vol. *263*, pp. 401–412.
[9] N. Eswara Prasad, A. Kumar, J. Subramanyam, *Aerospace Materials and Material Technologies*, (Eds: N. Prasad, R. Wanhill), Indian Institute of Metals Series. Springer, Singapore **2017**.
[10] E. Lutz, *J. Am. Ceram. Soc.* **1994**, *77*, 1274.
[11] S. R. Hay, E. G. Fair, T. Tidball, *J. Am. Ceram. Soc.* **2015**, *98*, 1907.
[12] M. Schmücker, P. Mechnich, *J. Am. Ceram. Soc.* **2008**, *91*, 1306.
[13] N. Siegel, M. Gross, C. Ho, C. T. Phan, J. Yuan, *Energy Proc.* **2014**, *49*, 1015.
[14] G. Alkan, P. Mechnich, H. Barbri, F. Flucht, D. Sergeev, M. Müller, in *Proc. 27th SolarPACES Conf.* online conference **2021**.
[15] R. Buck, C. Agrafiotis, S. Tescari, N. Neumann, M. Schmücker, *Front. Energy Res.* **2021**, *9*.
[16] P. Mechnich, G. Alkan, *Adv. Appl. Ceram.* **2023**.